PHYSICAL REVIEW E **79**, 036302 (2009)

Percolation and permeability of networks of heterogeneous fractures

H. Hamzehpour*
UPMC Sisyphe, Boîte 105, 4 place Jussieu, 75252 Paris cedex 05, France
and Department of Physics, K.N. Toosi University of Technology, 15875-4416 Tehran, Iran

V. V. Mourzenko† and J.-F. Thovert‡
LCD, SP2MI, BP 30179, 86962 Futuroscope Cedex

P. M. Adler§
UPMC Sisyphe, Boîte 105, 4 place Jussieu, 75252 Paris cedex 05, France

(Received 28 May 2008; published 10 March 2009)

Networks composed by heterogeneous fractures whose local permeability is a binary correlated random field are generated. The percolation and permeability properties of a single heterogeneous fracture are strongly influenced by finite size effects when the correlation length is of the order of the fracture size. For fracture networks, a mean-field approximation is derived which approximates well the macroscopic permeability while an empirical formula is proposed for the percolation properties.

DOI: 10.1103/PhysRevE.79.036302 PACS number(s): 47.56.+r, 91.60.Ba, 64.60.ah

I. INTRODUCTION

The determination of the macroscopic properties of fracture networks has generated a considerable fundamental and industrial interest since many applications are crucial for industries such as petroleum and waste storage.

Some general references can be given on this topic which summarize the knowledge accumulated over the years from different points of view such as [1–4]. Note that the solid medium located in between the fractures is supposed to be impermeable and that the classical double porosity approach [5] is not applicable here.

In all these studies and to the best of our knowledge, the fracture properties are assumed to be uniform and generally constant for the whole network. It is only in a few contributions (see, for instance, [6]) that the fracture permeability scales as a power law of the fracture lateral extent; however, the permeability is uniform over each fracture. It should be noted that early studies [7,8] pointed out the channelization of the flow, i.e., its division into separate channels or equivalently the existence of extended zones where the fracture aperture is equal to zero. Surprisingly, this feature has never been taken into account at the network level though it may significantly influence the macroscopic properties.

Therefore, it is the major purpose of the present paper to address this point. In order to simplify the physical situation, the fracture local permeability will only take two values, namely 0 and σ_o. The percolation threshold and the macroscopic permeability of networks of heterogeneous fractures which may be locally open or closed are studied in a systematic way. Such a binary approximation would probably not be valid for solute transport governed by a convection-diffusion equation. In this latter situation, the small aperture zones will induce long tails in the concentration plumes since they correspond to low velocity zones; therefore, the macroscopic dispersion tensor is likely to be drastically influenced by the aperture distribution. This approximation will be discussed further.

This paper is organized as follows. Section II describes the generation of the fractures and their binary approximation. Then, it shows how fracture networks are generated and it recalls briefly the meshing and the determination of the flow and of the percolation properties. Section III is devoted to the study of a single fracture and a detailed analysis of the parameters which govern the equations is made. Section IV contains the most important results of this paper since it is devoted to the properties of three-dimensional networks, i.e., percolation and permeability.

This paper is ended by some concluding remarks.

II. GENERAL

The fracture networks considered in this work are made up of plane polygonal fractures. These polygons may be regular or not, but all their vertices N_v (regular or random) are supposed to lie on a circumscribed circle whose radius R provides a measure of the lateral extension of the fractures. The local permeability $\sigma(\mathbf{x})$ of each fracture is supposed to take two values, namely 0 and σ_o; $\sigma(\mathbf{x})$ is a correlated random field as it will be seen below. Since $\sigma(\mathbf{x})$ corresponds to a flow rate per unit fracture width, $\sigma(\mathbf{x})$ is homogeneous to the cube of a length [2].

A. Generation of fracture networks

The network generator has been detailed by [9]. Plane polygonal fractures are inserted in a cell τ_0 of size L. Unless otherwise stated, the following properties hold throughout this paper. The fracture normal vectors $\mathbf{n}$ are randomly and isotropically distributed over the unit sphere and the fracture

---

*hossein.hamzehpour@ccr.jussieu.fr
†mourzenk@lcd.ensma.fr
‡thovert@lcd.ensma.fr
§pierre.adler@upmc.fr

centers obey a Poisson distribution. N_v and R are identical for all the fractures in the network. Therefore, a network is entirely characterized by a fracture shape (or equivalently N_v), the normalized cell size L/R, and the number of fractures per unit volume ρ. Only two shapes are studied in this paper, namely square when a single fracture is considered (Sec. III) and hexagonal when addressing three-dimensional (3D) networks (Sec. IV).

ρ can be expressed by using the excluded volume V_{ex} introduced by Balberg *et al.* [10]. For two objects 1 and 2, V_{ex} is defined as the volume surrounding object 1 into which the center of object 2 may not enter if overlap between 1 and 2 is to be avoided. For two equal convex polygons of area A and perimeter P, V_{ex} is equal to [2]

$$V_{ex} = \tfrac{1}{2}AP. \tag{1}$$

The dimensionless fracture density ρ' is defined as the number of fractures per excluded volume

$$\rho' = V_{ex}\rho. \tag{2}$$

It is also equal to the number of intersections per fracture [10].

B. Triangulation and permeability distribution

In order to solve the flow equation, the fracture network must be discretized. Since the fractures have polygonal shapes, possibly random, and intersect randomly, the most natural discretization is an unstructured triangulation. This triangulation must obey a few *a priori* constraints. All the original polygon vertices, intersection end points, and triple points (intersections of fractures intersections) must coincide with vertices of the triangular mesh; all the original polygon borderlines and fracture intersections must coincide with triangle edges; the triangulation of two intersecting fractures must match along their intersection line [11]. The sides of the triangles are of the order of (and generally smaller than) a given discretization length δ_M.

In our previous contributions [11–13], permeability was constant in each fracture. The present paper goes one step further by taking into account the fact that significant parts of real fractures have a zero aperture and therefore a zero permeability. Such parts are called the contact zone.

The two surfaces of a fracture can be described by their heights $z=h^{\pm}(x,y)$ above an arbitrary reference plane z, with a mean separation b_m. Usually, $h^{\pm}$ are assumed to be normally distributed random variables with a variance σ_h^2 [12]. The aperture b of the fracture is the difference $w=h^+-h^-$ when it is non-negative,

$$b = \begin{cases} w, & w(\boldsymbol{r}) \geqslant 0, \\ 0, & w(\boldsymbol{r}) < 0. \end{cases} \tag{3}$$

When w is negative, the surfaces are considered to be in contact, with $h^+=h^-$. As a consequence of the Gaussian character of the h^+ and h^-, the open fractional area ϵ the average aperture $\langle b\rangle_o$ over the void fracture area can be expressed as

$$\epsilon = \frac{1}{2}\,\mathrm{erf}\left(-\frac{b'_m}{2}\right), \tag{4a}$$

$$\frac{\langle b\rangle_o}{\sigma_h} = b'_m + \frac{2}{\pi^{1/2}}\exp\left(-\frac{b'^2_m}{4}\right)\frac{1}{\mathrm{erfc}\left(-\frac{b'_m}{2}\right)}, \tag{4b}$$

where $b'_m=b_m/\sigma_h$.

The statistical properties of the fracture in the xy plane can be characterized by the spatial covariance functions $C_{h^{\pm}}$ of the fields h^+ and h^-. These two functions are assumed to be identical, stationary, and isotropic. Hence, they reduce to the function $C_h(u)$ of the norm u of the lag $\mathbf{u}$,

$$C_h(u) = \langle[h^{\pm}(\mathbf{r}) - \langle h^{\pm}\rangle][h^{\pm}(\mathbf{r}+\mathbf{u}) - \langle h^{\pm}\rangle]\rangle. \tag{5}$$

The open surface corresponds to the zone $b>0$; equivalently, the correlated Gaussian field h^+-h^- is equal to zero. Therefore, the statistical generation of this open surface is equivalent to the generation of a phase function $Z(\mathbf{x})$ which is equal to 1 when the surface is open and zero otherwise. This phase function is statistically characterized by a probability ε and a correlation function $\mathcal{R}_Z(u)$,

$$\varepsilon = \overline{Z(\mathbf{x})}, \quad \mathcal{R}_Z(u) = \frac{\overline{[Z(\mathbf{x}) - \varepsilon][Z(\mathbf{x}+\mathbf{u}) - \varepsilon]}}{(\varepsilon - \varepsilon^2)}, \tag{6a}$$

where u is the norm of the translation vector $\mathbf{u}$. The overbar denotes the spatial average. $Z(\mathbf{x})$ is derived by thresholding a Gaussian field $Y(\mathbf{x})$ correlated by

$$\mathcal{R}_Y(u) = e^{-u^2/\ell_c^2}, \tag{6b}$$

where ℓ_c is the correlation length.

The present channel generation can now be precisely compared to the one used by [7]. Actually, the general methodology is exactly the same, but the generations differ by the choice of the input functions. Reference [7] generated log-normally distributed apertures, with exponentially decaying spatial covariances while here Gaussian distributed apertures with Gaussian decaying spatial covariances are generated and thresholded.

Two remarks should be made on the resulting fractures. First, it should be noticed that the choice of the distribution function does not have any influence when the apertures are later thresholded. Second, the choice of an exponential covariance implies that the resulting fractures are self-affine which is not the case for the Gaussian covariance; the exponential and the Gaussian covariances represent the two extremes of the general form introduced by [15]. The Gaussian covariance was preferred since it does not introduce any additional complication due to the fractal character.

Various ways exist to choose a constant permeability σ_o for the open zones of a fracture. A critical path analysis [14,16] might be used to justify a constant permeability σ_o for the open zones. A first physical approximation would consist in taking the fracture aperture as a constant and equal to $\langle b\rangle_o$. Then, σ_o can be estimated by the classical cubic law

$$\sigma_0 = \frac{\langle b\rangle_o{}^3}{12} \tag{7}$$

or by a fraction of this value [2]. The validity of this approximation will be further discussed in Sec. IV A 2.

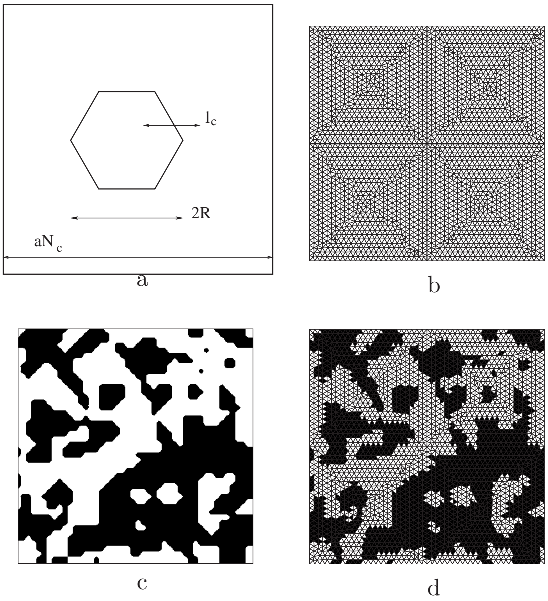

FIG. 1. Discretization of a fracture. (a) The length scales involved in the generation and discretization of a fracture. (b) A triangulated grid; (c) the field $Z(\mathbf{x})$ on the square grid; (d) the corresponding permeability distribution on the unstructured lattice. Color code for squares and triangles, white $[Z(\mathbf{x})=1]$, black $[Z(\mathbf{x})=0]$. The hexagonal fracture of size $2R$ shown in (a) is located at the center of the square of size aN_c in (c) and (d).

It is assumed that ε and ℓ_c are identical for all the fractures of the networks which are generated. When all the fractures of the network are triangulated, the discretization of each fracture is made in two steps. For each fracture i, a field $Z_i(\mathbf{x})$ is generated on a square grid $N_c \times N_c$ made of elementary squares of size a. $Z_i(\mathbf{x})$ is equal to 0 or 1 on each elementary square. The size aN_c of the square grid is usually chosen equal to or larger than $4R$.

The field $Z_i(\mathbf{x})$ is generated with periodic boundary conditions on the square grid. This necessitates (see [17]) that aN_c is larger than $2\ell_c$. This is illustrated in Fig. 1(a).

Once the field $Z_i(\mathbf{x})$ is generated, the fracture is discretized as follows. The center of the triangulated fracture of size $2R$ is arbitrarily located at the center of the square grid of size aN_c. It should be emphasized that the size of the fracture which is usually hexagonal is smaller than the size of the square grid on which the field $Z_i(\mathbf{x})$ is generated. For instance, the hexagonal fracture shown in Fig. 1(a) is located at the center of the squares displayed in Figs. 1(c) and 1(d). When the gravity center of a triangle belongs to a square with $Z_i=1$, the permeability of the corresponding triangle is equal to σ_o, and zero otherwise. Note that the fracture has been initially divided into four equal squares; the thick lines limiting these squares could correspond to intersections with other fractures of the network.

To summarize, this construction mode introduces five lengths, namely two physical lengths R and ℓ_c, and three artificial lengths δ_M, a, and aN_c. a is generally taken equal to δ_M in order that the dimensions of the squares and the triangles are comparable.

Figure 2 illustrates the influence of the triangular grid, of ε and of the correlation length ℓ_c on the local permeability field in square fractures. Of course, the results look very much alike the porous media generated by the same technique [17]. The two parameters ε and ℓ_c have exactly the same influence as on porous media. It is also clear that the exact nature of the triangular grid made of equilateral triangles (for the hexagonal lattices) and of triangles of arbitrary shapes (for the unstructured lattices) is very limited.

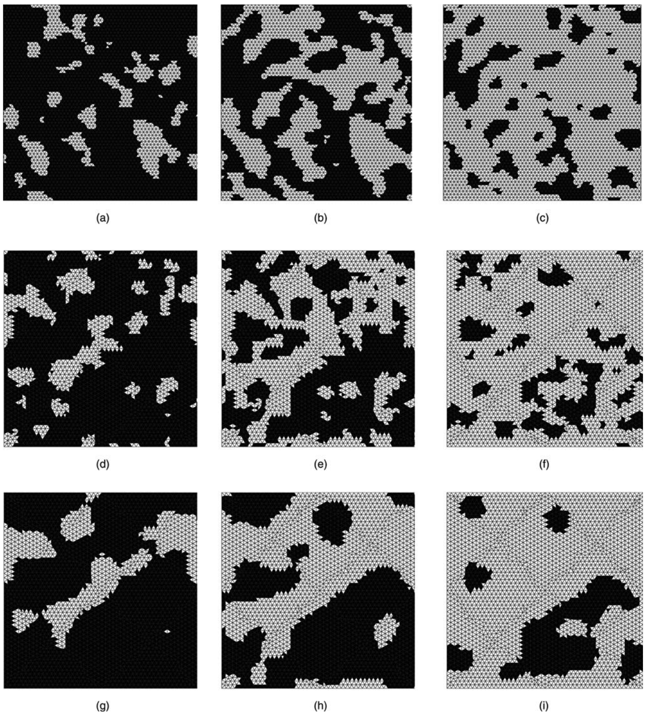

FIG. 2. A square fracture discretized on a hexagonal lattice with $\varepsilon=0.2$ (a), 0.5 (b), and 0.8 (c) and discretized on an unstructured triangle lattice in (d), (e), and (f), respectively; $\ell_c=0.177L_2$ where L_2 is the fracture side. For the same values of ε and $\ell_c=0.354L_2$, fractures (g), (h), and (i) are discretized on an unstructured lattice.

The permeability of each fracture of the network can be discretized by the same method, once it is triangulated. Of course, the field $Z(\mathbf{x})$ is generated independently for each fracture.

The qualitative influence of ε and of ρ is shown in Fig. 3. Two fractures may intersect, but in order that fluid can flow from one to another, it is necessary that the open zones of each fracture overlap in some sense along the intersections; otherwise, the two fractures are not connected when flow is considered. More precisely, consider an intersection between two fractures. This intersection is divided into segments which are the sides of triangles contained in one of the two intersecting fractures. Fluid can flow from one fracture to the other if two triangles with permeability σ_o belonging to the two fractures have at least one node in common. Of course, this is not sufficient in the sense that these two triangles should also belong to the percolating cluster.

Therefore, when the network of fractures of constant permeability σ_o percolates for a given fracture density ρ, one can determine the minimal value ε_c for which the network of heterogeneous fractures percolates; ε_c is expected to be a decreasing function of ρ. This phenomenon and its consequences are detailed in Sec. IV B 2.

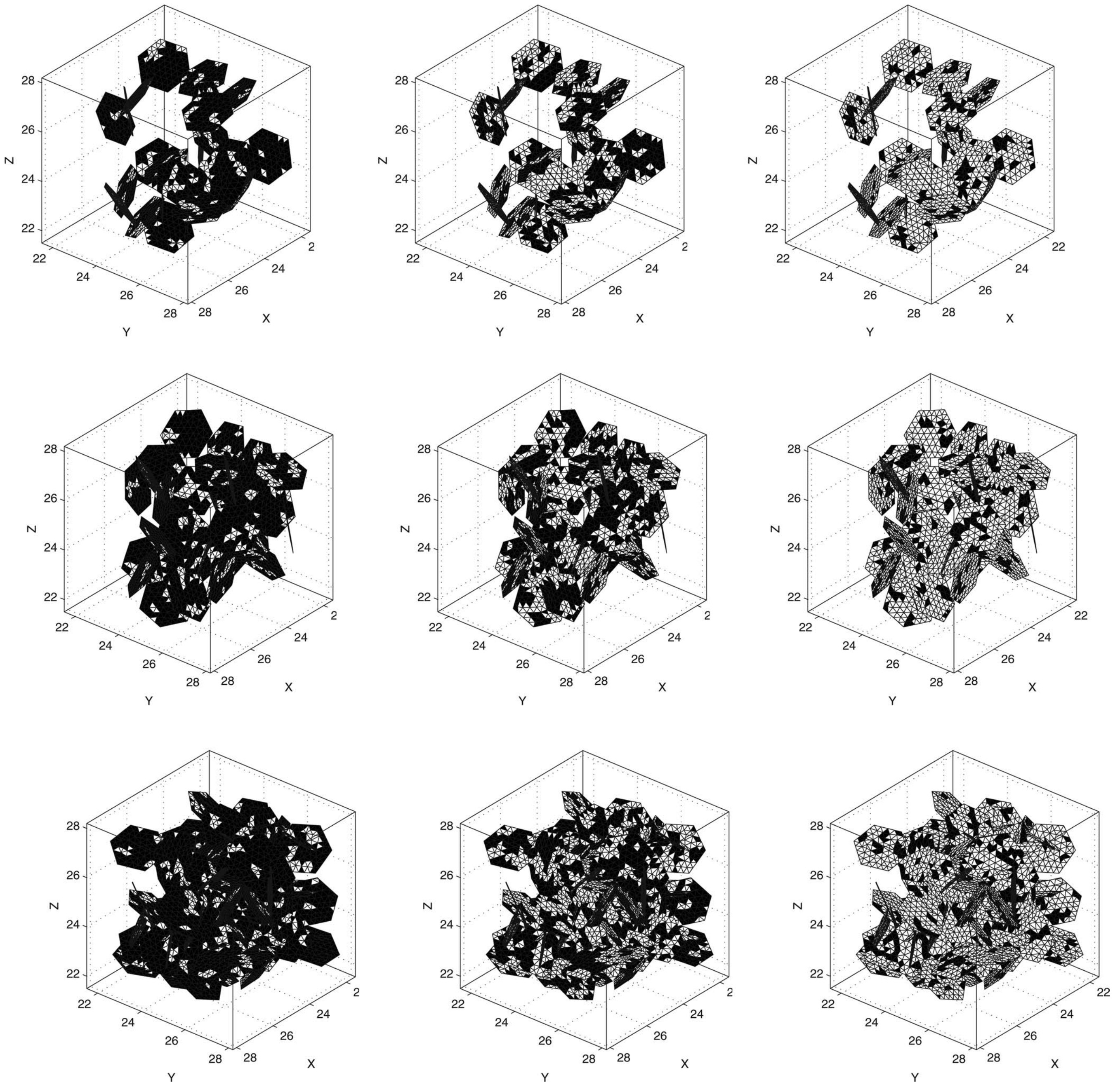

FIG. 3. Influence of ρ' and ε on fracture networks. $\ell_c/R=0.5$ and $L/R=5$. Each line corresponds to a given value of ρ'; from top to bottom, $\rho'=1.5, 2.3, 5.6$. Each column corresponds to a given value of ε; from left to right, $\varepsilon=0.2, 0.5, 0.8$.

The previous developments apply to fractures which belong to a network. The discretization of a single fracture is given in Sec. III.

C. Flow equations

Typically, flow is determined in cubic unit cells of size L such as the ones displayed in Fig. 3. The solid matrix containing the fractures is assumed to be impermeable. On a local scale characterized by a typical aperture $\langle b \rangle_0$ [cf. (9)], the flow of a Newtonian fluid at low Reynolds number within a fracture is governed by the Stokes equation. If $\langle b \rangle_0$ is assumed to be much smaller than the typical lateral extent $2R$ of the fracture, the flow on scales intermediate between b_0 and $2R$ is governed by the Darcy equation

$$\mathbf{q}' = -\frac{1}{\mu'}\sigma' \overline{\boldsymbol{\nabla}' p'}, \tag{8}$$

where $\mathbf{q}'$ is the local flow rate per unit width $[L^2T^{-1}]$, μ' the fluid viscosity, $\overline{\boldsymbol{\nabla}' p'}$ the pressure gradient, and $\sigma'[L^3]$ is the fracture conductivity. All of the dimensional quantities related to fluid and flow are denoted by a prime. Mass conservation implies

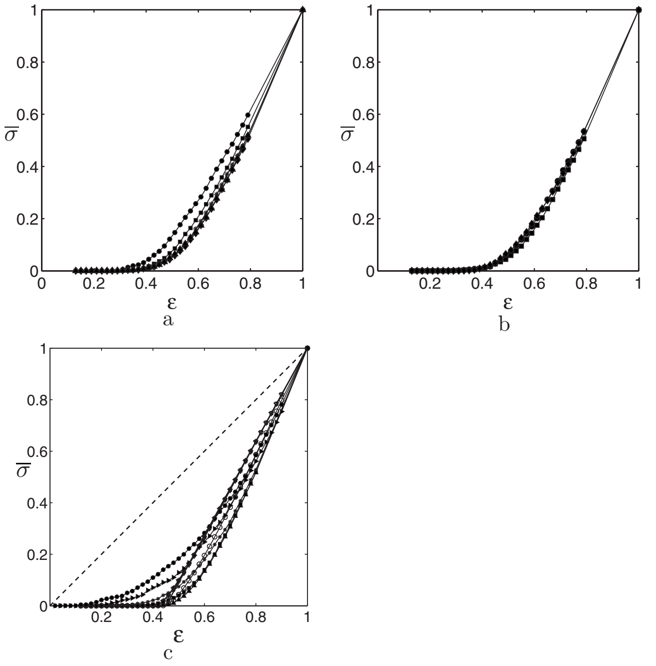

FIG. 4. The average macroscopic dimensionless permeability $\bar{\sigma}$ as a function of ε for a single fracture discretized by unstructured triangles. ℓ_c/L_2=0.177. (a) Influence of δ_M/L_2; data are for δ_M/L_2=0.088 (●), 0.044 (■), 0.022 (◆), 0.011 (*), 0.0055 (▲). (b) Influence of a/δ_M; data are for δ_M/L_2=0.022; a/δ_M=0.5 (●), 1 (■), 2 (◆). (c) Influence of ℓ_c/L_2; data are for ℓ_c/L_2=0 (▽), 0.01 (▽), 0.05 (○), 0.0885 (▲), 0.177 (■), 0.354 (*), 0.71 (▶), 1 (●). δ_M/L_2=0.0055; the broken line is the limit $\bar{\sigma}=\varepsilon$ for $\ell_c/L_2 \to \infty$; the solid line is the fit by (17).

$$\nabla_s' \cdot \mathbf{q}' = 0, \tag{9}$$

where ∇_s' is the two-dimensional gradient operator in the mean fracture plane.

The boundary conditions which supplement Eqs. (8) and (9) are of three types. First, the flow normal to the fracture external boundaries should vanish. Second, at fracture intersections, pressure should be equal and fluxes conserved. Third, periodic boundary conditions are applied on the local flux $\mathbf{q}'$ and for $\overline{\nabla' p'}$.

In addition, the driving force of the flow is an overall pressure gradient $\overline{\overline{\nabla' p'}}$ which can be expressed as

$$\overline{\overline{\nabla' p'}} = \frac{1}{\tau_0} \int_{\partial \tau_0} p' d\mathbf{s}'. \tag{10}$$

The seepage velocity $\overline{\mathbf{v}'}$ can be evaluated as

$$\overline{\mathbf{v}'} = \frac{1}{\tau_0} \int_{\tau_f} \mathbf{v}' d\tau' = \frac{1}{\tau_0} \int_{S_f} \mathbf{q}' ds', \tag{11}$$

where τ_f is the interstitial volume of the fractures and S_f their projection on their mean planes. The flux is related to the pressure gradient by Darcy's law [2]

$$\overline{\mathbf{v}'} = -\frac{1}{\mu'} \mathbf{K}' \cdot \overline{\overline{\nabla' p'}}. \tag{12}$$

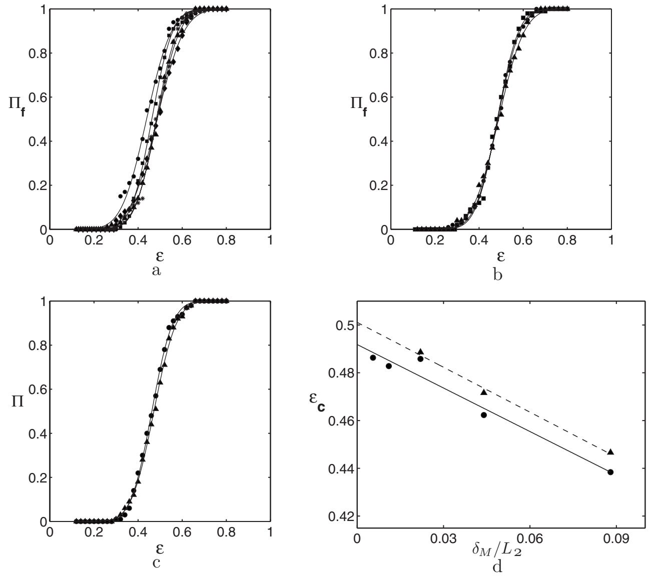

FIG. 5. The percolation probability Π_f as a function of ε for a single fracture discretized by unstructured triangles; Π_f is derived from the macroscopic permeability. Conventions are the same as in Fig. 4(a). ℓ_c/L_2=0.177. (a) Influence of δ_M/L_2. (b) Influence of a/δ_M for δ_M/L_2=0.011. (c) Comparison of the percolation probabilities Π_g (▲) and Π_f (●); δ_M=0.044L_2. (d) ε_c as a function of δ_M/L_2 derived from geometry (▲) and from flow (●) for a single fracture meshed by unstructured triangles.

$\mathbf{K}'$ is the permeability tensor $[L^2]$ to be determined from Eqs. (11) and (12), once Eqs. (8) and (9) are solved. The dimensionless permeability is defined as

$$\mathbf{K} = \frac{R}{\sigma_0} \mathbf{K}'. \tag{13}$$

Since the fields Z_i and the fracture distribution in space are isotropic, $\mathbf{K}$ is reduced to a spherical tensor $K\mathbf{I}$ where K is the scalar permeability and $\mathbf{I}$ is the unit tensor.

The discretization and resolution of (9) can be summarized as follows. Equation (9) is integrated over nonoverlapping domains Ω_m that surround each node m of the triangles. Denote by $T_m(t)$, $t=1,\ldots,n_m$ the n_m triangles whose one node is m. If the node belongs to the intersection of two or three fractures, Ω_m is simply the union of the two or three domains obtained in each fracture as indicated above. Finally, by a systematic use of the divergence theorem, a discretized conservation equation is obtained around each node m. This equation involves p_m and all the pressures at the nodes of the triangles $\{T_m(t), t=1,\ldots,n_m\}$. These equations for all the nodes can be summarized by the linear system

$$\mathbf{A} \cdot \mathbf{p} = \mathbf{B}, \tag{14}$$

where $\mathbf{p}$ is the vector whose components are the pressures at all the nodes, $\mathbf{B}$ a vector which corresponds to the driving force, i.e., to the macroscopic pressure gradient. It is easily shown that the matrix $\mathbf{A}$ depends only on the geometry of the triangles and that it is symmetric. This matrix is also large and sparse, but shows no organization since the triangular grid is unstructured. Therefore, the most efficient storage

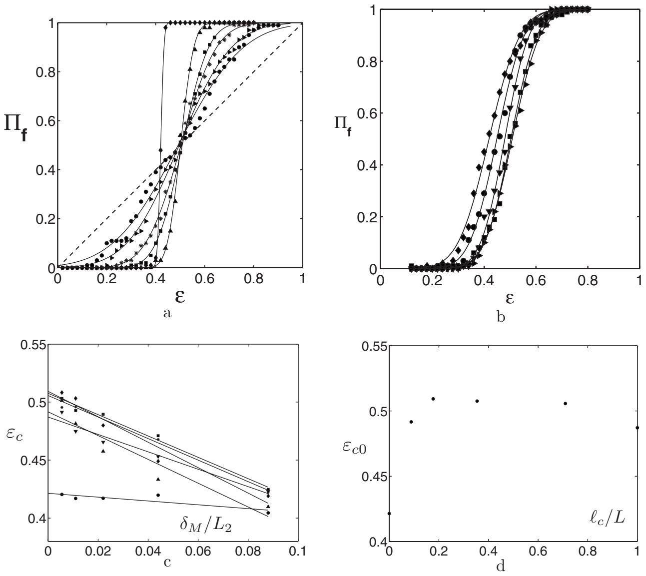

FIG. 6. (a) The percolation probability Π_f as a function of ε for a single fracture discretized by unstructured triangles for various values of ℓ_c/L_2. Conventions are the same as in Fig. 4(c). The broken line is the limit $\Pi_f=\varepsilon$ for $\ell_c/L_2 \to \infty$. (b) The percolation probability Π_f as a function of ε for a single fracture discretized by unstructured triangles with $\ell_c/L_2=0.177$; data are for $\delta_M/L_2=0.088$ (◆), 0.044 (●), 0.022 (▼), 0.011 (■), 0.0055 (▶). (c) ε_c as a function of δ_M/L_2 for a single fracture discretized by unstructured triangles for various values of ℓ_c/L_2. Data are for $\ell_c/L_2=0$ (●), 0.0885 (▲), 0.177 (◆), 0.354 (■), 0.71 (*), 1 (▼). (d) The extrapolated percolation threshold ε_{c0} for a single fracture discretized by unstructured triangles as a function of ℓ_c/L_2.

mode is to record the coefficients of the pressure p_m at node m in the discretized conservation equation for each triangle of the network. The balance equation for each grid point is built by summing the contributions from all its incident triangles. The resulting system is solved by a classical conjugate gradient technique.

D. Percolation

Since one of the purposes of this paper is to determine the percolation threshold $\varepsilon_c(\rho')$ of the fracture network as a function of the density ρ', it is important to detail how the percolation of a given fracture or of a given network is calculated.

There are many ways which can be used in order to determine the percolation properties of a set, one of them being the Hoshen-Kopelman algorithm [18]. Here, two ways based on numerical tools which are available are used to study the percolation property, either by purely geometric considerations or by solving the flow equation.

The first method can be explained for a single fracture since it is easily extended to 3D. The easiest way is to introduce the adjacency matrix $\mathbf{A}$ of the permeable triangles. The matrix element A_{ij} is equal to 1 if the two triangles i and j have at least one common node. The size of this matrix is $N_t \times N_t$, where N_t is the total number of triangles in the fracture. The percolation of a single fracture from its left-hand side $x=0$ to its right-hand side $x=L_2$ can be studied as follows. Introduce the vector $\mathbf{T}_0$ (with N_t lines) whose elements are 1 for permeable triangles which have at least one node with $x=0$, and 0 otherwise. Then, it is an easy matter to realize that the triangles connected to this set correspond to the nonzero elements of the vector $\mathbf{T_1}=\mathbf{A}\cdot\mathbf{T_0}$. This multiplication can be repeated until the resulting vector $\mathbf{T_n}$ is constant; more precisely, at each step $\mathbf{T_{m+1}}=\mathbf{A}\cdot\mathbf{T_m}$ is replaced by a vector composed of 0 and 1 only. Then, one can check if $\mathbf{T_n}$ contains a permeable triangle with at least one node with $x=L_2$. If it does, the network percolates. Obviously, this method is straightforward to implement and not costly from a numerical point of view.

The calculations are done for N_r independent realizations of the network for each value of ε. The value of N_r in two dimensions (2D) is 100, and in 3D is 50. The average of the N_r realizations provides the percolation probability $\Pi_g(\varepsilon)$ as a function of the probability ε.

The second method to obtain the percolation probability function is to solve the flow equations. The fracture percolates when K is not equal to 0. Again this calculation is performed on N_r realizations. The time necessary to solve the flow equation is remarkably low and it is smaller than the time needed for the geometrical method. The percolation probability $\Pi_f(\varepsilon)$ is derived from the flow calculation by generating as before N_r independent realizations of the network for each value of ε.

In both cases, the percolation probability $\Pi_\alpha(\varepsilon)$ $(\alpha=g,f)$ is fitted by an error function of the form

$$\Pi_\alpha(\varepsilon) = \frac{1}{\sqrt{2\pi}}\int_{-\infty}^{\varepsilon} \frac{1}{\Delta_\alpha} \exp\left(-\frac{(\xi-\varepsilon_{\alpha c})^2}{2\Delta_\alpha^2}\right) d\xi, \quad \alpha=g,f, \tag{15}$$

where $\varepsilon_{\alpha c}$ is the critical threshold and Δ_α is the width of the transition region of $\Pi_\alpha(\varepsilon)$.

III. RESULTS FOR A SINGLE FRACTURE

In this section, percolation and flow are studied in a single square fracture such as the ones displayed in Fig. 2. In contrast with the hexagonal fractures generated for networks, the single fracture is square with periodic boundary conditions. The side L_2 of the fracture is equal to the side of the unit cell. The fracture is triangulated once for all since it does not intersect any other fracture. The field $Z(\mathbf{x})$ which verifies (6a) and (6b) is generated and the permeability of each triangle is determined according to the value of $Z(\mathbf{x})$ at its center of gravity.

Since the lengths necessary to describe the fracture are δ_M, a, ℓ_c, and L_2, the average macroscopic dimensionless permeability $\bar{\sigma}$ of a single fracture averaged over N_r independent realizations depends on four parameters

$$\bar{\sigma} = \frac{1}{N_r}\sum_{i=1}^{N_r}\frac{\sigma_i}{\sigma_0} = \bar{\sigma}(\varepsilon, \ell_c/L_2, \delta_M/L_2, a/\delta_M), \tag{16a}$$

where σ_i is the macroscopic permeability of the ith fracture.

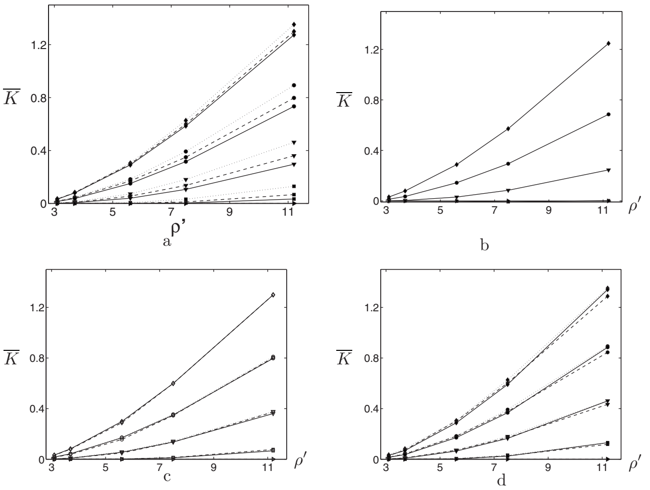

FIG. 7. Influence of the artificial parameters on the average macroscopic permeability $\bar{K}$. $\ell_c/R=0.5$ and $L/R=5$. (a) $\bar{K}$ as a function of ρ' for various values of ε with $\delta_M/R=\frac{1}{4}$ (dotted lines), $\frac{1}{8}$ (broken lines), $\frac{1}{16}$ (solid lines). (b) $\bar{K}$ as a function of ρ' for various values of ε with δ_M/R extrapolated to 0. In (a) and (b), data are for $\varepsilon=1$ (♦), 0.8 (●), 0.6 (▼), 0.4 (■), and 0.2 (▶). (c) and (d), $\bar{K}$ as a function of a/δ_M (c) and L/R (d). (c) Data are for $a/\delta_M=0.5$(⋯), 1(—) and 2(- - -); $\varepsilon=1$ (♦), 0.8 (●), 0.6 (▼), 0.4 (■) and 0.2 (▶). $\delta_M/R=\frac{1}{8}$, $L/R=5$. (d) Data are for $\delta_M/R=\frac{1}{4}$; $\varepsilon=1$ (♦), 0.8 (●), 0.6 (▼), 0.4 (■), and 0.2 (▶); $L/R=5$ (⋯), 8(- - -), and 10(—).

The percolation threshold ε_c can be written as

$$\varepsilon_c(\ell_c/L_2,\delta_M/L_2,a/\delta_M). \tag{16b}$$

Of course, δ_M/L_2 and a/δ_M are artificial parameters which should disappear from the final results.

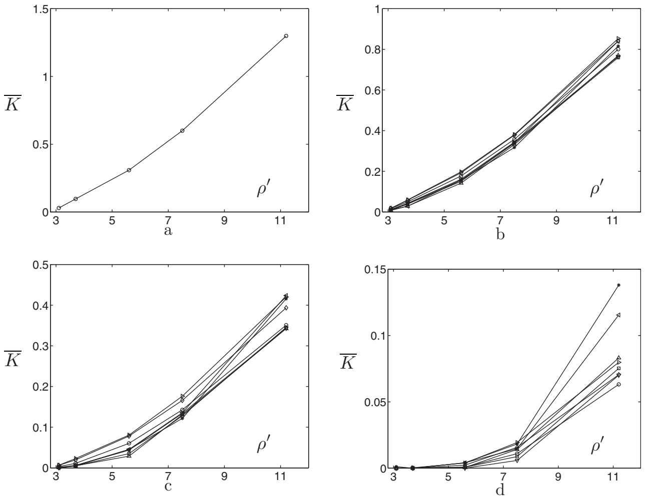

FIG. 8. Influence of the ratio ℓ_c/R on the macroscopic permeability $\bar{K}$. Data are for $\varepsilon=1$ (a), 0.8 (b), 0.6 (c), and 0.4 (d); $\ell_c/R=0$ (▷), $\frac{1}{8}$ (◇), $\frac{1}{2}$ (○), 1 (▽), $\frac{3}{2}$ (□), 2 (△), 5 (△), 10 (*). $\delta_M/R=\frac{1}{8}$.

In the following, the square single fracture is triangulated by unstructured triangles using the general advancing front technique.

A. Permeability

First, in order to check the influence of δ_M/L_2 and a/δ_M, calculations are done for various values of these parameters. The permeability distribution is correlated by the Gaussian field (6b) with $\ell_c/L_2=0.177$. Periodic boundary conditions are applied along both x and y directions, but the average pressure gradient is parallel to the x axis.

Since percolation properties are often derived from flow calculations, it might be easier to start with the data related to $\bar{\sigma}$.

The influence of the artificial parameters δ_M/L_2 and a/δ_M on $\bar{\sigma}$ is summarized in Fig. 4. Figure 4(a) displays the macroscopic permeability $\bar{\sigma}$ averaged over 100 independent realizations as a function of ε for a single fracture discretized by unstructured triangles for different values of δ_M/L_2. When δ_M/L_2 is equal to 0.088, 0.044, 0.022, 0.011, and 0.0055, the number of triangles in the fracture is equal to 384, 1464, 5160, 20248, and 79416, respectively. As expected, $\bar{\sigma}$ tends towards a limit for small values of δ_M/L_2. The differences between the various values of δ_M/L_2 are very small when $\delta_M/L_2 \leqslant 0.022$.

For these values of δ_M/L_2, systematic calculations were performed for three values of $a/\delta_M=0.5$, 1, and 2 in order to estimate the influence of this parameter. The results obtained for $\delta_M/L_2=0.022$ are displayed in Fig. 4(b); this corresponds to the largest influence of a/δ_M and it is seen to be very limited.

Systematic calculations were performed for $\delta_M/L_2=0.0055$ and are presented in Fig. 4(c) for various values of the correlation length ℓ_c. $\bar{\sigma}(\varepsilon,\ell_c/L_2)$ is varying between two known limits. When ℓ_c/L_2 is large, the fracture permeability is equal to σ_0 with a probability ε, and 0 otherwise; therefore, $\bar{\sigma}$ is equal to ε. When ℓ_c/L_2 is small (and even 0), this corresponds to the classical site percolation where the values of the triangles are independent from one another. This graph is interesting since the evolution of $\bar{\sigma}$ is nonuniform with ℓ_c/L_2 for a given value of ε. When ℓ_c/L_2 decreases from 1 to approximately 0.0885, a minimal curve is obtained; when ℓ_c/L_2 is further decreased, $\bar{\sigma}$ increases. For $\ell_c/L_2=0$, a linear relation is obtained which can be fitted by

$$\bar{\sigma}(\varepsilon,0) \approx 1.814\varepsilon - 0.814. \tag{17}$$

The agreement with the numerical data is excellent, except of course close to percolation.

In order to make sure that this nonuniform behavior is not due to the triangular mesh, similar calculations were made on the classical square mesh which was binarized as detailed in Sec. II B; similar results were obtained. A last check was performed for $\ell_c/L_2=0$; instead of using the machinery described in Sec. II B, a classical site percolation was devised with a random number generator; again similar results were obtained.

Another remark should be made. For an infinite fracture, the correlation length ℓ_c does not play any role as soon as it

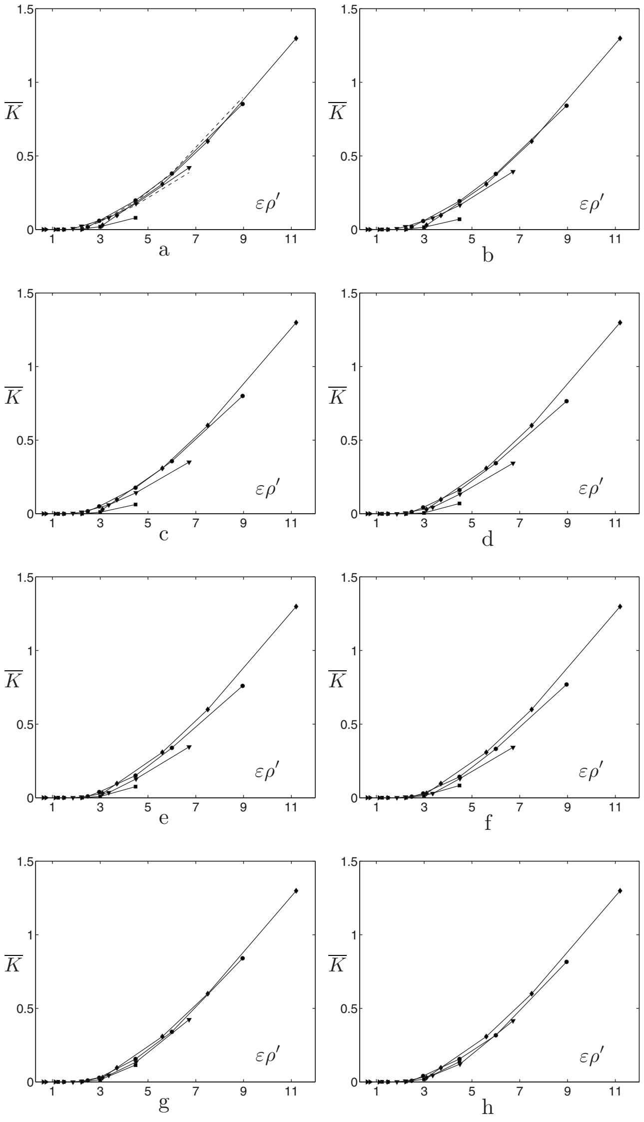

FIG. 9. Influence of the ratio ℓ_c/R on $\bar{K}$ as a function of $\varepsilon\rho'$, with $\varepsilon=1$ (◆), 0.8 (●), 0.6 (▼), 0.4 (■) and 0.2 (▶). Data are for $\ell_c/R=0$ (a), $\frac{1}{8}$ (b), $\frac{1}{2}$ (c), 1 (d), $\frac{3}{2}$ (e), 2 (f), 5 (g), and 10 (h). $\delta_M/R=\frac{1}{8}$. In (a), the broken lines correspond to the combination of (20) and of (17).

is not zero. Of course, the artificial ratio ℓ_c/a describes the discretization, but it should be chosen large enough in order that the discretization effects are negligible.

This discussion can be concluded by noting that the variations displayed in Fig. 4 correspond to the so-called finite-size effects [19] and are usually eliminated by finite-size scaling. Here, these effects correspond to real physical ingredients since ℓ_c may well be of the order of magnitude of the fracture size.

B. Percolation

Let us now turn to the percolation properties. As explained in Sec. II D, the percolation probability function can be derived from flow calculations. In Fig. 5(a), the percolation probability Π_f is shown as a function of ε for a single fracture discretized by unstructured triangles for various values of δ_M/L_2. The simulated data are fitted by the error function (15). The resulting values for ε_c and Δ are given in Table I. Again it is clear that ε_c tends towards a limit when δ_M/L_2 tends towards 0.

TABLE I. ε_c and Δ as functions of δ_M/L in a single fracture triangulated by an unstructured mesh derived from flow and geometry calculations. $\ell_c/L=0.177$.

	$\frac{\delta_M}{L_2}$	ε_c	Δ
Flow	0.088	0.4384	0.1261
	0.044	0.4623	0.1056
	0.022	0.4858	0.1369
	0.011	0.4828	0.1077
	0.0055	0.4863	0.1140
	0	0.4918	
Geometry	0.088	0.4466	0.1561
	0.044	0.4716	0.1136
	0.022	0.4886	0.1313
	0	0.5011	

The influence of the second artificial parameter a/δ_M was determined for $\delta_M/L_2=0.022$, 0.011, and 0.0055. As it was noticed in the preceding section for permeability, the influence of a/δ_M is an increasing function of δ_M/L_2. Only the intermediate case is displayed in Fig. 5(b); it is seen that again the role of this artificial parameter is very limited.

The percolation threshold was also derived by the geometrical method. In this case, nonperiodic boundary conditions are used. The corresponding percolation probability function Π_g is very similar to Π_f as it can be seen in Fig. 5(c). The resulting values for ε_c and Δ are given in Table I.

Since the computational times increase with decreasing δ_M, the smallest value used for percolation is $\delta_M/L_2=0.022$. Π_g and Π_f are practically identical for small values of δ_M.

These preliminary results on the percolation properties can be summarized by saying that the two techniques give very close results and that the role of a/δ_M is decreasing when δ_M/L_2 decreases.

In order to eliminate the artificial parameter δ_M, the data should be extrapolated for $\delta_M/L_2=0$. This extrapolation is illustrated in Fig. 5(d) and the extrapolated values ε_{co} are given in Table I. The values of ε_{co} using Π_f and Π_g are 0.4918 and 0.5011, respectively; therefore, these values are very close which gives some confidence in the derivation of the threshold by means of flow calculations.

Once these methodological preliminaries are made, the role of the parameter ℓ_c/L_2 can be analyzed. It is interesting to provide the probability curves $\Pi_f(\varepsilon,\ell_c/L_2)$ in Fig. 6(a). When the correlation length increases, Π_f becomes less steep around the percolation threshold. In the limit $\ell_c/L_2\rightarrow\infty$, Π_f is equal to ε for the same reasons as for $\bar{\sigma}$ [see Fig. 4(c)]. This progressive smoothing of $\Pi_f(\varepsilon,\ell_c/L_2)$ around ε_c is again analogous to the well-known finite-size effect [19]. Close to the percolation threshold, the cluster size is diverg-

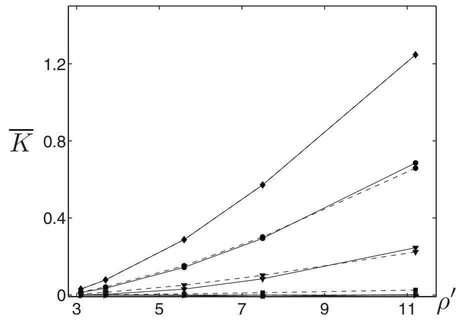

FIG. 10. Comparison of the mean-field approximation with the results obtained using the solving flow equation as in Fig. 7(d). The dashed lines correspond to the mean-field approximation. Data are for $\varepsilon=1$ (◆), 0.8 (●), 0.6 (▼), 0.4 (■), and 0.2 (▶). $\ell_c/R=0.5$ and $L/R=5$.

ing and becomes of the same order of magnitude as the size of the cell. More precisely, the basic dimension of the elements is ℓ_c; in the limit $\ell_c=0$, the curve $\Pi_f(\varepsilon)$ is relatively steep since δ_M/L_2 is small; when ℓ_c is comparable to the fracture size, the curve becomes smooth.

The percolation probability Π_f was systematically determined as a function of ε for $\delta_M/L_2=0.088$, 0.044, 0.022, 0.011, and 0.0055 for each value of ℓ_c/L_2. The values of ℓ_c/L_2 were 0.0885, 0.177, 0.354, 0.71, and 1; an example is displayed in Fig. 6(b). When these curves are fitted by (15), ε_c is obtained as a function of δ_M/L_2 for each ratio ℓ_c/L_2; the results are shown in Fig. 6(c); these curves can be extrapolated for $\delta_M/L_2=0$ and the corresponding value ε_{c0} of the threshold is obtained for each ratio ℓ_c/L_2. The extrapolated percolation threshold ε_{c0} is displayed as a function of ℓ_c/L_2 in Fig. 6(d); except for $\ell_c/L_2=0$, it is very close to 0.5.

The value $\varepsilon_{c0}=0.5$ is indeed expected for continuous correlated two-dimensional binary media, since percolation of one phase along a given direction prevents the existence of a connected path in the other phase along the transverse direction. Symmetry imposes that $\varepsilon_c=1/2$. Moreover, the percolation threshold does not depend on the correlation length since a change in ℓ_c corresponds simply to a scale change. These arguments apply for any nonpathological correlation function (e.g., differentiable), but they may fail in a discretized representation. For instance, it is possible that two connected paths through the two phases intersect at a node of a triangular mesh and this may decrease ε_c. This effect is observed here for coarse meshes, but as expected, it becomes negligible when the discretization step δ_M becomes small compared to the correlation length ℓ_c. More details on percolation thresholds in two-dimensional correlated media can be found in [20].

Finally, some of these calculations were repeated for a single fracture discretized by equilateral triangles. The results were very similar to the ones obtained for unstructured triangles.

IV. RESULTS FOR FRACTURE NETWORKS

In this section, 3D networks made up of monodisperse hexagonal fractures are studied. When compared to the two-dimensional permeability (16a), the macroscopic dimensionless three-dimensional permeability K is expected to depend on two additional parameters, namely the fracture density ρ' and the ratio L/R between the cell size L and the fracture radius R; this is summarized by the formula

$$K=\frac{K'R}{\sigma}=K(\rho',\varepsilon,\ell_c/R,a/\delta_M,L/R,\delta_M/R). \tag{18a}$$

Only the first three parameters are physically meaningful. The last three ones are artificial and are introduced for the numerical calculations only. The same comments can be made about percolation and the percolation threshold ε_c is written as [cf. (16b)]

$$\varepsilon_c(\rho',\ell_c/R,\delta_M/R,L/R,a/\delta_M). \tag{18b}$$

Since the percolation properties are derived from the flow properties, we start by presenting the results relative to permeability.

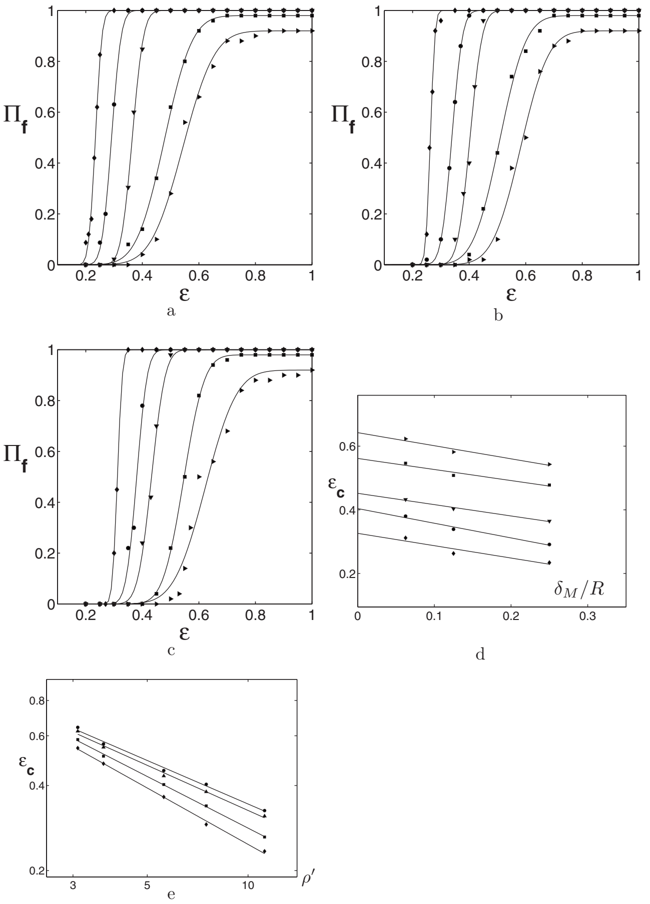

FIG. 11. Influence of δ_M/R on the percolation threshold in three dimensions. $\ell_c/R=0.5$ and $L/R=5$. (a, b, c) Π_f as a function of ε for various ρ' values with $\delta_M/R=\frac{1}{4}$ (a), $\frac{1}{8}$ (b), and $\frac{1}{16}$ (c). Data are for $\rho'=3.1$ (▶), 3.7 (■), 5.6 (▼), 7.5 (●), and 11.2 (◆). (d) ε_c as a function of δ_M/R for various values of ρ', obtained using the results of (a, b, c). Same conventions as in (a, b, c). (e) ε_c as a function of ρ' in a logarithmic plot, for various values of δ_M/R. Data are for $\delta_M/R=\frac{1}{4}$ (◆), $\frac{1}{8}$ (■), $\frac{1}{16}$, (▲), and 0 (●). The data for $\delta_M/R=0$ have been deduced from (d).

A. Permeability

It is necessary to note that this study will not address the properties of permeability close to the percolation threshold. Moreover, the mean value $\bar{K}$ of the permeability over 50 configurations is always considered in this Subsection.

1. Influence of the artificial parameters

Let us start with the artificial parameters δ_M/R, a/δ_M, and L/R. It will be seen that the influence of these parameters is coupled in the sense that the influence of one of them may depend on the influence of the others.

The first important parameter is the ratio δ_M/R which compares the mesh size to the fracture size. The two other parameters a/δ_M and L/R are equal to 1 and 5, respectively. An intermediate value 0.5 was given to the correlation length ℓ_c/R.

$\bar{K}$ is displayed in Fig. 7(a) as a function of ρ' for a fixed value of ε and for three values of δ_M/R. $\bar{K}$ is an increasing function of δ_M/R; note that the differences between $\delta_M/R=1/8$ and $1/16$ for $\rho'=11$ is always of the order of 0.05.

Therefore, these data need to be extrapolated for $\delta_M/R=0$. The corresponding curves in arithmetic plots are shown in Fig. 7(b). This figure corresponds to the representation of the data which could be possibly used for practical applications; the curves could be used as master curves to predict the network permeability when the two parameters ρ' and ε are known. $\bar{K}$ is an increasing function of ρ' and ε as it is obvious intuitively.

Let us now consider the influence of the second artificial parameter a/δ_M which has been briefly studied and the results are illustrated in Fig. 7(c). As for the two-dimensional case [cf. Fig. 4(b)], its influence is seen to be very limited.

The last artificial parameter is the ratio L/R. Three values were selected: $L/R=5$, 8, and 10. Moreover, for each of these values, δ_M/R was equal to $1/4$ and $1/8$. It is interesting to note that the role of L/R decreases with δ_M/R (and reversely); this provides an example of the coupled influence of the artificial parameters which was previously mentioned. The data for $\delta_M/R=1/4$ are illustrated in Fig. 7(d). They confirm that far from the percolation threshold the influence of the cell size L on K is very limited.

This preliminary study of the artificial parameters leads to the following conclusions. The data need to be extrapolated to $\delta_M/R=0$; the influence of L/R on the permeability is sufficiently small and the calculations can be limited to $L/R=5$.

2. Influence of the physical parameters

Let us return to the study of the physical parameters. The roles of ε and ρ' have already been sketched in Fig. 7(b).

The last important parameter is the ratio ℓ_c/R which compares the correlation length to the fracture size. The limit $\ell_c/R=0$ corresponds to site percolation where the permeability σ_0 of each triangle is chosen independently of its neighbors. The other limit $\ell_c/R=\infty$ is simpler; each fracture has a uniform permeability which is equal either to 0 or σ_0; therefore, $\bar{K}$ is expected to depend only on the product $\varepsilon\rho'$ in this limit.

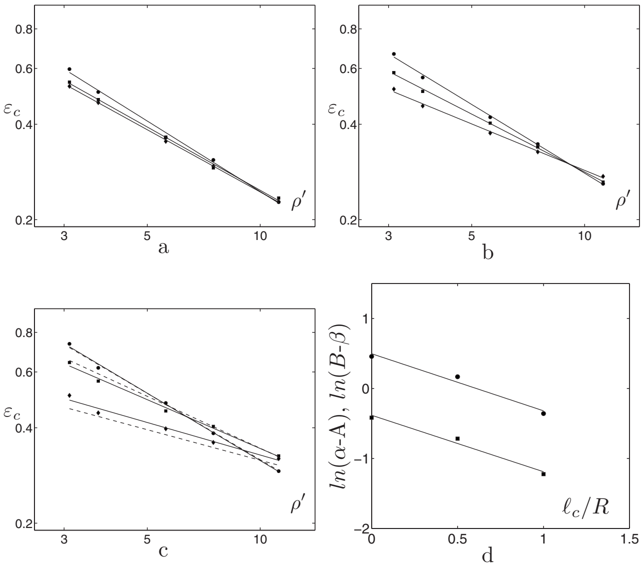

FIG. 12. Influence of ℓ_c/R on the percolation threshold for $L/R=5$. (a, b, c) ε_c as a function of ρ' in a logarithmic plots, for various values of $\delta_M/R=\frac{1}{4}$ (a), $\frac{1}{8}$ (b), and 0 (c); data are for $\ell_c/R=0$ (◆), 0.5 (■), and 1 (●); the broken lines in (c) correspond to (23) and (24). (d) $\ln(\alpha-A)$ (■) and $\ln(B-\beta)$ (●) as functions of ℓ_c/R with $A=-1$ and $B=2.3$.

A complete set of data is given in Fig. 8. These data which represent a significant amount of numerical calculations have been restricted to an intermediate grid size $\delta_M/R=1/8$. The influence of ℓ_c/R on $\bar{K}$ is relatively limited and it diminishes when ε increases. In the worst case, for $\varepsilon=0.4$, $\bar{K}$ for $\ell_c/R=\infty$ is less than 3 times larger than for $\ell_c/R=0$. It should be noticed that the limiting case $\ell_c/R=0$ is somewhat singular in agreement with the results for a single fracture [see Fig. 4(c) and the related discussion].

The limit $\ell_c/R=\infty$ can be better understood by plotting all the data as functions of $\varepsilon\rho'$ in Fig. 9. The results are quite remarkable since they are always very close to the classical curve obtained for $\varepsilon=1$. A closer look shows that the deviations from this curve are maximal for intermediate values of ℓ_c/R. In other words, it is only when ℓ_c is of the order of R that the deviations are important.

It might be the right place to detail the application of a mean field approximation [21] to the determination of the macroscopic permeability $\bar{K}$. In this type of approximation, each fracture is replaced by a fracture whose permeability is $\bar{\sigma}(\varepsilon,\ell_c/R)$ as given for instance by Fig. 4(c). The macroscopic dimensionless permeability of a network with fractures of permeability σ_0 is given by

$$K_0=\frac{\sigma_0}{R}f(\rho'). \tag{19a}$$

The dimensionless permeability $f(\rho')$ of a monodisperse network with fractures of a constant permeability can be approximated by the power law based on numerical results given by [11]

$$f(\rho')\approx 0.0455(\rho'-\rho'_c)^{1.57}. \tag{19b}$$

TABLE II. Values of ρ', ε_c, and Δ for various δ_M/R in fracture networks.

	$\frac{\delta_M}{R}=\frac{1}{4}$		$\frac{\delta_M}{R}=\frac{1}{8}$		$\frac{\delta_M}{R}=\frac{1}{16}$		$\frac{\delta_M}{R}=0$
ρ'	ε_c	Δ	ε_c	Δ	ε_c	Δ	ε_{co}
3.1	0.5429	0.1256	0.5818	0.1108	0.6230	0.1237	0.6425
3.7	0.4779	0.1097	0.5081	0.1037	0.5463	0.0817	0.5614
5.6	0.3644	0.4460	0.4032	0.0484	0.4325	0.0543	0.4519
7.5	0.2912	0.0379	0.3389	0.0420	0.3801	0.0419	0.4040
11.2	0.2340	0.0260	0.2629	0.0180	0.3117	0.0196	0.3262

Therefore, the mean-field approximation for a network with fractures of permeability $\bar{\sigma}$ is simply

$$K=\frac{RK'}{\sigma_0}=\bar{\sigma}(\varepsilon,\ell_c/R)f(\rho'). \tag{20}$$

This approximation is verified in Fig. 10 for the extrapolated values of permeability obtained with $\ell_c/R=0.5$. Therefore, even in this intermediate range of values for ℓ_c/L, a very good agreement with the full numerical results is obtained as soon as ε is large enough.

This approximation is exact in the limit $\ell_c/R=\infty$. One can show that it also holds for $\ell_c/R=0$. The curve obtained for a single fracture in this limit in Fig. 4(c) can be approximated by (17). This last expression can be combined with (20). It is compared with the full numerical data in Fig. 9(a). The agreement is seen to be very good for the range of parameters which were studied. Again the mean-field approximation is well justified in this limit at least far from the percolation threshold since the fracture size R is large when compared to the size δ_M of the elements.

Since the two limit cases $\ell_c/R=0$ and ∞ obey the mean-field approximation, the agreement between the numerical data and this approximation as a function of $\varepsilon\rho'$ remains relatively good for all values of ℓ_c/R.

The success of this mean-field approximation is quite remarkable since the binarization of permeability creates complex channels which must be present along the same segment at a fracture intersection in order to connect the two fractures.

Therefore, the extension of the classical laws to the present case is a very interesting feature from theoretical and practical points of view. Moreover, because of the success of this mean-field approximation, it is anticipated that a continuous distribution of permeabilities inside the fractures will not yield a significantly different result.

B. Percolation

Percolation properties have been exclusively studied by solving the flow equations since this method is much more efficient than the geometrical algorithm as noticed in Sec. II D.

1. Influence of the artificial parameters

Again let us start with the artificial parameters a/δ_M, δ_M/R, and L/R. a/δ_M was shown in Sec. III B to have a very limited influence on the percolation properties of a single fracture; therefore, its influence on the percolation properties of a fracture network is expected to be also very limited.

The second important parameter is the ratio δ_M/R whose influence is illustrated in Fig. 11. the probabilities in (a,b,c) are fitted by the error function (15) in order to get the value of the percolation threshold ε_c and the standard deviation Δ_ε.

Of course, ε_c depends on δ_M/R as shown by Fig. 11(d). Therefore, the second step consists in the extrapolation of the data for $\delta_M/R=0$ in order to obtain ε_{co}. These calculations were repeated for several values of ρ'; the dependence of ε_c on δ_M/R does not seem to depend on ρ' in the sense that all the curves are parallel in Fig. 11(d). The results relative to ε_c and ε_{co} are gathered in Table II.

The third parameter is the ratio L/R which has only been briefly studied. Calculations were limited to $L/R=5$ and 10 with various values of δ_M/R. The differences were always limited to 5%.

2. Influence of the physical parameters

Let us study now the two physical parameters ρ' and ℓ_c/R.

It is important to stress the fact that ε_c depends on ρ'. This can be easily understood since percolation of a network depends on two conditions. First, the fracture network should percolate, i.e., $\rho'>\rho'_c\approx 2.3$. Second, the zones where the local permeability is not zero in two intersecting fractures should be in contact one with another. This second condition is more often met in a network when ρ' increases. Therefore, ε_c should be a decreasing function of ρ'; this feature is indeed observed in Fig. 11(e). The same is also true for the extrapolated values ε_{co}.

ε_{co} should also depend on the second physical parameter ℓ_c/R. The study of this dependence necessitates to restart the numerical calculations for various values of this parameter; networks are generated with various densities ρ', meshed with various values of δ_M/R; the resulting data are extrapolated to zero. This important numerical effort yields the function

$$\varepsilon_{co}=\varepsilon_{co}(\rho',\ell_c/R). \tag{21}$$

The limit $\ell_c/R=\infty$ is known since the network is composed of conducting fractures with a spatial density $\varepsilon\rho'$; therefore, the former result of [9] can be used to derive the expression

$$\varepsilon_{co} = 2.3\rho'^{-1} \quad \text{for } \ell_c/R = \infty. \tag{22}$$

In addition to this known limit, two other values were selected for ℓ_c/R, namely 0 and 1. The major data and the intermediate steps are the same as for Fig. 11. All these data are gathered and displayed in a slightly different way in Fig. 12. As already noticed, the potential user will tend to use the function defined by (21). A tentative semiempirical law which has no theoretical background can be proposed in order to synthetize the data

$$\varepsilon_c = \beta\rho'^{\alpha}, \tag{23}$$

where β and α are parameters which depend on ℓ_c/R. When (22) is used, α and β can be expressed as

$$\alpha = -1 + 0.68e^{-0.81(l_c/R)}, \tag{24a}$$

$$\beta = 2.3 - 1.65e^{-0.82(l_c/R)}. \tag{24b}$$

The fits are shown in Fig. 12(d).

The predictions of (23) where α and β are expressed by (24) are compared to the numerical data in Fig. 12(c). The agreement between the fits and the numerical data is seen to be good.

V. CONCLUDING REMARKS

The macroscopic properties of networks of heterogeneous fractures were systematically studied as functions of the network density, of the probability ε and of the correlation length which characterizes the heterogeneities in the fractures.

Master curves could be derived for the network macroscopic permeability. It was shown that a mean-field approximation where each fracture is replaced by a fracture with the average permeability corresponding to ε yields a first good approximation, at least far from the percolation threshold.

The threshold of the probability ε is shown to depend on the fracture density and on the correlation length. An empirical relation is given to describe the variations of the threshold as a function of these two variables.

This study can be extended in many ways. First, there is some theoretical interest to study the phenomena close to the percolation threshold in a detailed way.

Second, the distribution of the local permeability inside the fractures could be continuous instead of being binary. This extension is very important for practical purposes though the percolation properties will not be modified. It should be very interesting to check the validity of the mean-field approximation for various permeability distributions. The influence of these distributions on the macroscopic dispersion tensor will also be of a high interest.

---

[1] M. Sahimi, *Flow and Transport in Porous Media and Fractured Rock* (VCH, New York, 1995).

[2] P. M. Adler and J.-F. Thovert, *Fractures and Fracture Networks* (Kluwer Academic, Dordrecht, Netherlands, 1999).

[3] E. Bonnet, O. Bour, N. E. Odling, P. Davy, I. Main, P. Cowie, and B. Berkowitz, Rev. Geophys. **39**, 347 (2001).

[4] B. Berkowitz, Adv. Water Resour. **25**, 861 (2002).

[5] G. I. Barenblatt, I. P. Zheltov, and I. N. Kochina, J. Appl. Math. Mech. **24**, 852 (1960).

[6] V. V. Mourzenko, J.-F. Thovert, and P. M. Adler, Phys. Rev. E **69**, 066307 (2004).

[7] L. Moreno, Y. W. Tsang, C. F. Tsang, F. V. Hale, and I. Neretnieks, Water Resour. Res. **24**, 2033 (1988).

[8] Y. W. Tsang and C. F. Tsang, Water Resour. Res. **25**, 2076 (1989).

[9] O. Huseby, J.-F. Thovert, and P. M. Adler, J. Phys. A **30**, 1415 (1997).

[10] I. Balberg, C. H. Anderson, S. Alexander, and N. Wagner, Phys. Rev. B **30**, 3933 (1984).

[11] V. V. Mourzenko, J.-F. Thovert, and P. M. Adler, Phys. Rev. E **53**, 5606 (1996).

[12] V. V. Mourzenko, J.-F. Thovert, and P. M. Adler, Phys. Rev. E **72**, 036103 (2005).

[13] I. I. Bogdanov, V. V. Mourzenko, J.-F. Thovert, and P. M. Adler, Phys. Rev. E **76**, 036309 (2007).

[14] V. Ambegaokar, B. I. Halperin, and J. S. Langer, Phys. Rev. B **4**, 2612 (1971).

[15] S. K. Sinha, E. B. Sirota, S. Garoff, and H. B. Stanley, Phys. Rev. B **38**, 2297 (1988).

[16] S. P. Friedman, Water Resour. Res. **34**, 1703 (1998).

[17] P. M. Adler, C. G. Jacquin, and J. A. Quiblier, Int. J. Multiphase Flow **16**, 691 (1990).

[18] J. Hoshen and R. Kopelman, Phys. Rev. B **14**, 3438 (1976).

[19] M. E. Fischer, "The theory of critical point singularities," in *Critical Phenomena*, edited by M. S. Green, Proceedings of the 51st Fermi School, Varenna, Italy (Academic, New York, 1971).

[20] V. V. Mourzenko, J.-F. Thovert, and P. M. Adler, Eur. Phys. J. B **19**, 75 (2001).

[21] S. Kirkpatrick, Phys. Rev. Lett. **27**, 1722 (1971).